DATA REPOSITORY ITEM 2015123

General Geology

Great Basin Region (NV) – Shingle Pass, Antelope Range, and Meiklejohn Peak

The depositional environment of the Great Basin region during the Ordovician was a passive margin carbonate ramp with intermittent influxes of siliciclastic sediment (Ross et al., 1989). The oldest rocks sampled in this study are from the Pogonip Group and are earliest Ordovician (Tremadocian) in age based on the conodont faunas present (Sweet and Tolbert, 1997; Fig. 3). The Pogonip Group contains, from base to top, the House Limestone, Parker Spring Formation, Shingle Limestone, Kanosh Shale, and Lehman Formation, which are overlain by the Middle-Upper Ordovician Eureka Quartzite (Kellogg, 1963; Ross et al., 1989). The Middle Ordovician lithostratigraphic units (Shingle Limestone to Lehman Formation) differ in the Antelope Range and Meiklejohn Peak sections and are known as the Antelope Valley Limestone and Copenhagen Formation, which is also overlain by the Eureka Quartzite (Figs. 3 and 4). Carbonate lithologies range from sparsely fossiliferous micrite with minor amounts of siliciclastic silt and clay grains (e.g., House Limestone) to fossiliferous wackestone-packstone beds (Antelope Valley Limestone, Shingle Limestone), sometimes interbedded with laminae to thin beds of siliciclastic mudstone (Parker Spring, Copenhagen Formation, Lehman Formation) (Ross, 1970; Ross and Shaw, 1972; Young et al. 2009; Edwards and Saltzman, 2014). Conodonts from the Great Basin region range in alteration from the least altered in the Antelope Range (CAI: 1-2), to moderate at Shingle Pass (CAI: 3-4.5), to the most altered in this study at Meiklejohn Peak (CAI: up to 5) (Harris et al., 1979; Sweet and Tolbert, 1997).

Arbuckle Mountains, Oklahoma

The Middle-Upper Ordovician Simpson Group is exposed along roadcuts of Interstate-35, US-77, and US-99 in the Arbuckle Mountains in south-central Oklahoma (Bauer, 1987, 1994, 2010). The Simpson Group contains a mixed succession of siliciclastic quartz sandstone, siltstone, and shale interbedded with massive to well-bedded limestone, which ranges from micritic mudstone to coarse-grained grainstone (Fay, 1989; Derby et al. 1991). The oldest formation of the Simpson Group is the Joins, which is overlain by the Oil Creek, McLish, Tulip Creek, and Bromide formations (Fig. 5). During the Middle Ordovician, sedimentation along the Southern Oklahoma Embayment is interpreted to have occurred on a carbonate ramp along a rifted margin, possibly the conjugate margin of the Argentine Precordillera (Thomas and Astini, 1996; Albanesi and Bergström, 2010). Conodonts from the Simpson Group are some of the least thermally altered conodonts sampled in this study and yield CAI values of 1-2.

Appalachian Region – Clear Spring (MD), Rocky Gap (VA), Interstate-81 (VA), Roaring Spring – Union Furnace (Central PA)

The Paleozoic strata in the Appalachian Region have been folded and faulted during the Appalachian Orogeny and subsequent erosion has exposed numerous sections of Ordovician strata that contain a wide range of lithologies. The Clear Spring section is an excellent exposure of Ordovician strata located along an Interstate-70 roadcut in the Valley and Ridge Province of central Maryland (Fig. 1). The section includes the upper portion of the Beekmantown Group, the entire St. Paul Group, and the lower portion of the Chambersburg Limestone (Leslie et al., 2011; Brezinski et al., 2012; Fig. DR2). The Beekmantown Group comprises well-bedded lime micrite of the Rockdale Run Formation and cyclic thin-medium beds of dolomitic lithologies of the Pinesburg Station Dolomite interpreted by Brezinski et al. (2012) to have accumulated in a restricted tidal flat environment.

The Rocky Gap section is exposed along a roadcut of Interstate-77 in southwestern VA (Fig. 1), the base of which is recognized as the massively bedded Knox Dolomite. The upper contact of the Knox Dolomite is an erosional surface with locally present karstic features and has been studied in detail for its significance in recording changes in sea level and tectonics in the Appalachian basin (Mussman and Read, 1986; Read and Eriksson, 2012). Known as the Knox Unconformity, this surface is recognized throughout the Appalachian basin from northern Virginia south to Alabama and is interpreted to record a sea level lowstand that represents the boundary between the Sauk-Tippecanoe megasequences (Brezinski et al., 1999; Brezinski et al., 2012). This surface is also recognized in the I-81 section (near Strasburg, VA) where karstic features are present (Leslie et al., 2011). In central Pennsylvania, the Beekmantown Group/Knox Dolomite is recognized as the Bellefonte Dolomite.

Overlying the Beekmantown Group in the Clear Spring section is the St. Paul Group. The base of the St. Paul Group is comprised of massive fenestral limestone and dolomites of the Row Park Formation and transitions into laminated lime- and dolo-micrite with stromatolitic beds near the base of the New Market Formation. At the Interstate-81 section only a few meters of this fenestral micritic limestone of the New Market Formation is present (Leslie et al., 2011). The New Market Formation and overlying Chambersburg Limestone are interpreted to reflect a relative deepening of the basin with more open marine circulation based on the increasing abundance of argillaceous and fossiliferous wackestone. In the Rocky Gap section, a portion of the St. Paul Group is recognized as the Elway Formation, a chert nodule-bearing limestone at its base that grades into an argillaceous limestone into the overlying Benbolt and Witten formations

(Fig. 7). Similar lithologies are present at the Roaring Spring-Union Furnace section (central PA) where age-equivalent strata are represented by basal wackestone-grainstone lithologies of the Loysburg Formation, up through the thick-bedded lime mudstone-wackestone lithologies of the Nealmont Formation interpreted to record deposition in deeper facies (see Laughrey et al. (2004) for a more detailed description of bed-by-bed lithologies and paleoenvironmental interpretation of these units).

Conodonts from the Appalachian Basin have experienced a moderate amount of thermal alteration, and conodont elements have CAI values between 3 and 5.

Methods

Variation of bulk rock dissolution methods

Because variations in Sr concentration of bulk carbonate and burial temperature as inferred from conodont alteration index (CAI) do not always predict $\Delta^{87}Sr/^{86}Sr$, we have evaluated the importance of sample preparation, dissolution, and insoluble residues. Three bulk carbonate samples with a range of $\Delta^{87}Sr/^{86}Sr$ values from the Shingle Pass section were selected to test how variations in the methods used to isolate carbonate-associated Sr may affect the $^{87}Sr/^{86}Sr$ (Tables DR4 and DR6).

A selection of eight insoluble residues from the bulk carbonate samples (Table DR6) was digested in a strong acid solution to document the end member of radiogenic $^{87}Sr/^{86}Sr$ values from siliciclastic material that may have been a source for post-burial isotopic exchange (cf. Bailey et al., 2000). An acidic solution of 29M HF (80%), 6N HNO_3 (10%), and 6N HCl (10%) was added to residues in sealed Teflon beakers, which were placed on a hotplate for several days until completely dissolved. Aliquots of Sr from dissolved residues were separated using the same cation exchange resin described in the main text.

Pre-leaching of conodonts

To test the effects of how a pre-leach step might affect the measured radiogenic $^{87}Sr/^{86}Sr$ value (cf. Ruppel et al., 1996; John et al., 2008), a small subset of six conodonts from three localities was selected (Table DR6). Following the methods of John et al. (2008), conodonts were rinsed in 0.5% acetic acid overnight to dissolve the outer layer of apatite. The leachate was removed to a spiked beaker and Sr was separated using the cation exchange resin. The leached conodonts were then dissolved in 6N HCl using the same procedure used in the main study.

Scanning electron microscopy

Two brachiopods were imaged using scanning electron microscopy to document how the microstructural preservation of these samples compared to their $^{87}Sr/^{86}Sr$ values. One sample was selected that had little apparent recrystallization (SP-165.5) and one that had some possible signs of alteration (B-2739; Table DR3). Samples were sputter coated in a Au-Pd alloy and imaged using an FEI Quanta Field Emission Gun scanning electron microscope housed in the Subsurface Energy Materials Characterization and Analysis Lab (SEM-CAL) at The Ohio State University. A beam intensity of 15 kV and spot size of 4 mm were used for imaging.

Results

Variations of bulk carbonate methods

We sought to test whether the measured $^{87}Sr/^{86}Sr$ ratio was contaminated by secondary Sr sourced from pore fluids or radiogenic clay minerals present in the powdered samples. Variations in the treatment of these bulk carbonate samples (see Methods section) only reduced the $^{87}Sr/^{86}Sr$ value by at most 0.000088 compared to the sample with no ammonium acetate or pre-leach steps. In none of the methods was the amount of pre-treatment or pre-leaching able to lower $^{87}Sr/^{86}Sr_{carb}$ values to the $^{87}Sr/^{86}Sr_{seawater}$ trend, suggesting that the highly radiogenic $^{87}Sr/^{86}Sr_{carb}$ values do record a diagenetic signature and are not artifacts of sample preparation. The $^{87}Sr/^{86}Sr$ of the insoluble residue fractions were also measured to determine if these residues may have contributed to highly radiogenic $^{87}Sr/^{86}Sr$ values, but the results are inconclusive (Fig. DR6) and require a more detailed investigation.

Scanning electron microscopy

Analysis of the brachiopod samples using scanning electron microscopy show a range of preservation of microstructures and secondary shell layers (Figs. DR4 and DR5). The secondary shell layers from sample SP-165.5 show well-preserved laminae with little evidence for recrystallization. However, the $^{87}Sr/^{86}Sr_{brach}$ value is significantly more radiogenic than the $^{87}Sr/^{86}Sr_{seawater}$ even though the microstructures appear to be pristine. The corresponding $^{87}Sr/^{86}Sr_{conodont}$ value is also significantly more radiogenic than the $^{87}Sr/^{86}Sr_{seawater}$ trend, suggesting that some degree of isotopic exchange occurred in both materials with the surrounding radiogenic red shaley limestone despite the lack of physical evidence of alteration. However, sample B-2739 has evidence of significant alteration with micro-vuggy porosity and a lack of well-defined secondary shell layers. Although the microstructure exhibits overall poor preservation, the $^{87}Sr/^{86}Sr_{brach}$ value is indistinguishable from corresponding $^{87}Sr/^{86}Sr_{conodont}$ values and is only slightly more radiogenic than the $^{87}Sr/^{86}Sr_{seawater}$ trend (0.000056; Fig. 6).

REFERENCES CITED

Albanesi, G.L., and Bergström, S.M., 2010, Early-Middle Ordovician conodont paleobiogeography with special regard to the geographic origin of the Argentine Precordillera: a multivariate data analysis: *in* Finney, S.C., and Berry, W.B.N., eds., The Ordovician Earth System: Geological Society of America Special Paper 466, p. 119-139.

Bailey, T.R., McArthur, J.M., Prince, H., and Thirlwall, M.F., 2000, Dissolution methods for strontium isotope stratigraphy: whole rock analysis: Chemical Geology, v. 167, p. 313-319.

Bauer, J.A., 1987, Conodonts and conodont biostratigraphy of the McLish and Tulip Creek Formations (Middle Ordovician), south-central Oklahoma: Oklahoma Geological Survey Bulletin, v. 141, 53 p.

Bauer, J.A., 1994, Conodonts from the Bromide Formation (Middle Ordovician), south-central Oklahoma: Journal of Paleontology, v. 68, p. 358-376.

Bauer, J.A., 2010, Conodonts and conodont biostratigraphy of the Joins and Oil Creek Formations, Arbuckle Mountains, South-central Oklahoma: Oklahoma Geological Survey Bulletin, v. 150, 44 p.

Brezinski, D.K., Repetski, J.E., and Taylor, J.F., 1999, Stratigraphic and paleontologic record of the Sauk III regression in the central Appalachians: National Park Service Paleontological Research, v. 3, p. 32-41.

Brezinski, D.K., Taylor, J.F., and Repetski, J.E., 2012, Sequential development of platform to off-platform facies of the Great American Carbonate Bank in the Central Appalachians, In: Derby, J.R., Fritz, R.D., Longacre, S.A., Morgan, W.A., and Sternbach, C.A. (Eds.), The great American carbonate bank: the geology and economic resources of the Cambrian-Ordovician Sauk megasequence of Laurentia, American Association of Petroleum Geologists Memoir, v. 98, p. 383-420.

Derby, J.R., Bauer, J.A., Miller, M.A., Creath, W.B., Repetski, J.E., Dresbach, R.I., Ethington, R.L., Loch, J.D., Stitt, J.H., Sweet, W.C., McHargue, T.R., Taylor, J.F., Miller, J.F., and Williams, M., 1991, Biostratigraphy of the Timbered Hills, Arbuckle, and Simpson Groups, Cambrian and Ordovician, Oklahoma: a review of correlation tools and techniques available to the explorationist: Oklahoma Geological Survey Circular, v. 92, p. 15-41.

Edwards, C.T., and Saltzman, M.R., 2014, Carbon isotope ($\delta^{13}C_{carb}$) stratigraphy of the Lower-Middle Ordovician (Tremadocian-Darriwilian) in the Great Basin, western United States: implications for global correlation: Palaeogeography, Palaeoclimatology, Palaeoecology, v. 399, p. 1-20.

Fay, R.O., 1989, Geology of the Arbuckle Mountains along Interstate 35, Carter and Murray counties, Oklahoma: Oklahoma Geological Survey Guidebook, v. 26, p. 1-50.

Harris, A.G., Bergström, S.M., Ethington, R.L., and Ross, R.J.Jr., 1979, Aspects of Middle and Upper Ordovician conodont biostratigraphy of carbonate facies in Nevada and southeast California and comparison with some Appalachian successions: Brigham Young University Geology Studies, v. 26, p. 7-33.

John, E.H., Cliff, R., and Wignall, P.B., 2008, A positive trend in seawater $^{87}Sr/^{86}Sr$ values over the Early-Middle Frasnian boundary (Late Devonian) recorded in well-preserved conodont elements from the Holy Cross Mountains, Poland: Palaeogeography, Palaeoclimatology, Palaeoecology, v. 269, p. 166-175.

Kellogg, H.E., 1963, Paleozoic stratigraphy of the Southern Egan Range, Nevada: Geological Society of America Bulletin, v. 74, p. 685-708.

Laughrey, C.D., and Kostelnik, J., Gold, D.P., Doden, A.G., and Harper, J.A., 2004, Trenton and Black River carbonates in the Union Furnace area of Blair and Huntingdon counties, Pennsylvania, *in* Pittsburgh, Pennsylvania, Pittsburgh Association of Petroleum Geologists Guidebook, 81 p.

Leslie, S.A., Saltzman, M.R., Bergström, S.M., Repetski, J.E., Howard, A., and Seward, A.M., 2011, Conodont biostratigraphy and stable isotope stratigraphy across the Ordovician Knox/Beekmantown unconformity in the central Appalachians, In: Gutiérrez-Marco, J.C., Rábano, I., and Diego, G.B. (Eds.), Ordovician of the World, Publicaciones del Instituto Geológico y Minero de España: Serie: Cuadernos del Museo Geominero, v. 14, p. 301-308.

Leslie, S.A., Repetski, J.E., Saltzman, M.R., Kaznosky, C.M., and Lizer, A.M., 2013, Conodont biostratigraphy of the Rockdale Run Formation, Pinesburg Station Dolomite, St. Paul Group, and Chambersburg Formation (Middle to Lower Upper Ordovician) near Clear Spring, Maryland: Geological Society of America Abstracts and Program, v. 45, p. 324.

Mussman, W.J., and Read, J.F., 1986, Sedimentology and development of a passive- to convergent-margin unconformity: Middle Ordovician Knox unconformity, Virginia Appalachians: Geological Society of America Bulletin, v. 97, p. 282-295.

Read, J.F., and Eriksson, K.A., 2012, Chapter 3: Paleozoic sedimentary successions of the Virginia Valley & Ridge and Plateau. The Geology of Virginia, p. 131-149.

Ross, R.J.Jr., 1970, Ordovician brachiopods, trilobites, and stratigraphy in eastern and central

Nevada: Geological Survey Professional Paper 639, 103 p.

Ross, R.J.Jr., and Shaw, F.C., 1972, Distribution of the Middle Ordovician Copenhagen Formation and its trilobites in Nevada: Geological Survey Professional Paper 749, 33 p.

Ross, R.J.Jr., James, N.P., Hintze, L.F., and Poole, F.G., 1989, Architecture and evolution of a Whiterockian (Early Middle Ordovician) carbonate platform, Basin Ranges of western U.S.A., In: Crevello, P.D., Wilson, J.L., Sarg, F., and Read, J.F., (Eds.), Controls on Carbonate Platform and Basin Development, Society of Economic Paleontologists and Mineralogists Special Publication No. 44, p. 167-185.

Ruppel, S.C., James, E.W., Barrick, J.E., Nowlan, G., and Uyeno, T.T., 1996, High-resolution $^{87}Sr/^{86}Sr$ chemostratigraphy of the Silurian: implications for event correlation and strontium flux: Geology, v. 24, p. 831-834.

Saltzman, M.R., Edwards, C.T., Leslie, S.A., Dwyer, G.S., Bauer, J.A., Repetski, J., Harris, A., and Bergström S.M., 2014, Calibration of a conodont apatite-based Ordovician $^{87}Sr/^{86}Sr$ curve to biostratigraphy and geochronology: implications for stratigraphic resolution: Geologic Society of America Bulletin, v. 126, p. 1551-1568.

Sweet, W.C., and Tolbert, C.M., 1997, An Ibexian (Lower Ordovician) reference section in the Southern Egan Range, Nevada, for a conodont-based chronostratigraphy. In: Taylor, M.E. (Ed.), Early Paleozoic Biochronology of the Great Basin, western United States, United States Geological Survey Professional Paper 1579, p. 51-84.

Thomas, W.A., and Astini, R.A., 1996, The Argentine Precordillera: a traveler from the Ouachita Embayment of North American Laurentia: Science, v. 273, p. 752-757.

Young, S.A., Saltzman, M.R., Foland, K.A., Linder, J.S., and Kump, L.R., 2009, A major drop in seawater $^{87}Sr/^{86}Sr$ during the Middle Ordovician (Darriwilian): links to volcanism and climate?: Geology, v. 37, p. 951-954.

Supplement Figure Captions:

Figure DR1. $^{87}Sr/^{86}Sr$ from bulk rock (this study) and conodont apatite (see Saltzman et al., 2014) from the Meiklejohn Peak section (Nevada). Conodont biostratigraphy from Harris et al. (1979). UO=Upper Ordovician. Gray circles indicate least altered bulk carbonate samples with [Sr] >300 ppm. The large offset between the $^{87}Sr/^{86}Sr_{seawater}$ curve and brachiopod data is attributed to the uncertainty in the ages assigned to $^{87}Sr/^{86}Sr_{conodont}$ values.

Figure DR2. $^{87}Sr/^{86}Sr$ from bulk rock (this study) and conodont apatite (see Saltzman et al., 2014) from the Clear Spring section (Maryland). Two $^{87}Sr/^{86}Sr_{carb}$ uncertainties are plotted where the uncertainty is wider than the width of the data point. Conodont biostratigraphy from Leslie et al. (2013). Gray circles indicate least altered bulk carbonate samples with >300 ppm Sr.

Figure DR3. $^{87}Sr/^{86}Sr$ from bulk rock and conodont apatite from the Interstate-81section (Virginia). Note that bulk carbonate $^{87}Sr/^{86}Sr$ measured from dolomite lithologies (dashed symbol lines) of the Beekmantown Formation are highly variable and significantly more radiogenic than corresponding conodont $^{87}Sr/^{86}Sr$. Conodont $^{87}Sr/^{86}Sr$ values do not change across the contact between the Beekmantown and New Market formations, suggesting that not much geologic time is missing in this locality compared to Rocky Gap, VA.

Figure DR4. Secondary electron image of the well-preserved secondary layer of brachiopod calcite (SP-165.5).

Figure DR5. Secondary electron image of the poorly preserve secondary layer of a brachiopod (B-2739) with vuggy porosity and the appearance of recrystallization along pore spaces.

Figure DR6. Conodont Sr concentrations versus CAI shows no significant correlation and that conodonts with high CAI values can contain about as much Sr as conodonts with the lowest CAI values.

Figure DR7. Cross plot of $\Delta^{87}Sr/^{86}Sr$ values versus the difference between the $^{87}Sr/^{86}Sr$ of eight insoluble residues and the corresponding $^{87}Sr/^{86}Sr_{seawater}$ value. There appears to be no correlation between highly radiogenic insoluble residues and highly altered bulk carbonates.

Figure DR8. Predicted changes in the Sr concentration (upper plots) of a limestone with 50% porosity, porefluid Sr/Ca ratio of 0.01, $D_{Sr} = 0.05$ (cf. Banner and Hanson, 1990), and [Ca] of the equilibrating fluid at increasing water:rock weight ratios (N) (Compare with Figure 8 of the main text). Also shown are the expected changes in the $^{87}Sr/^{86}Sr$ of a limestone with a fluid with a highly radiogenic $^{87}Sr/^{86}Sr$ value (0.7200; middle plots), and a fluid with a near-seawater $^{87}Sr/^{86}Sr$ value (lower plots).

Tables DR1–DR9 (2015123_TablesDR1-DR9.xlsx)

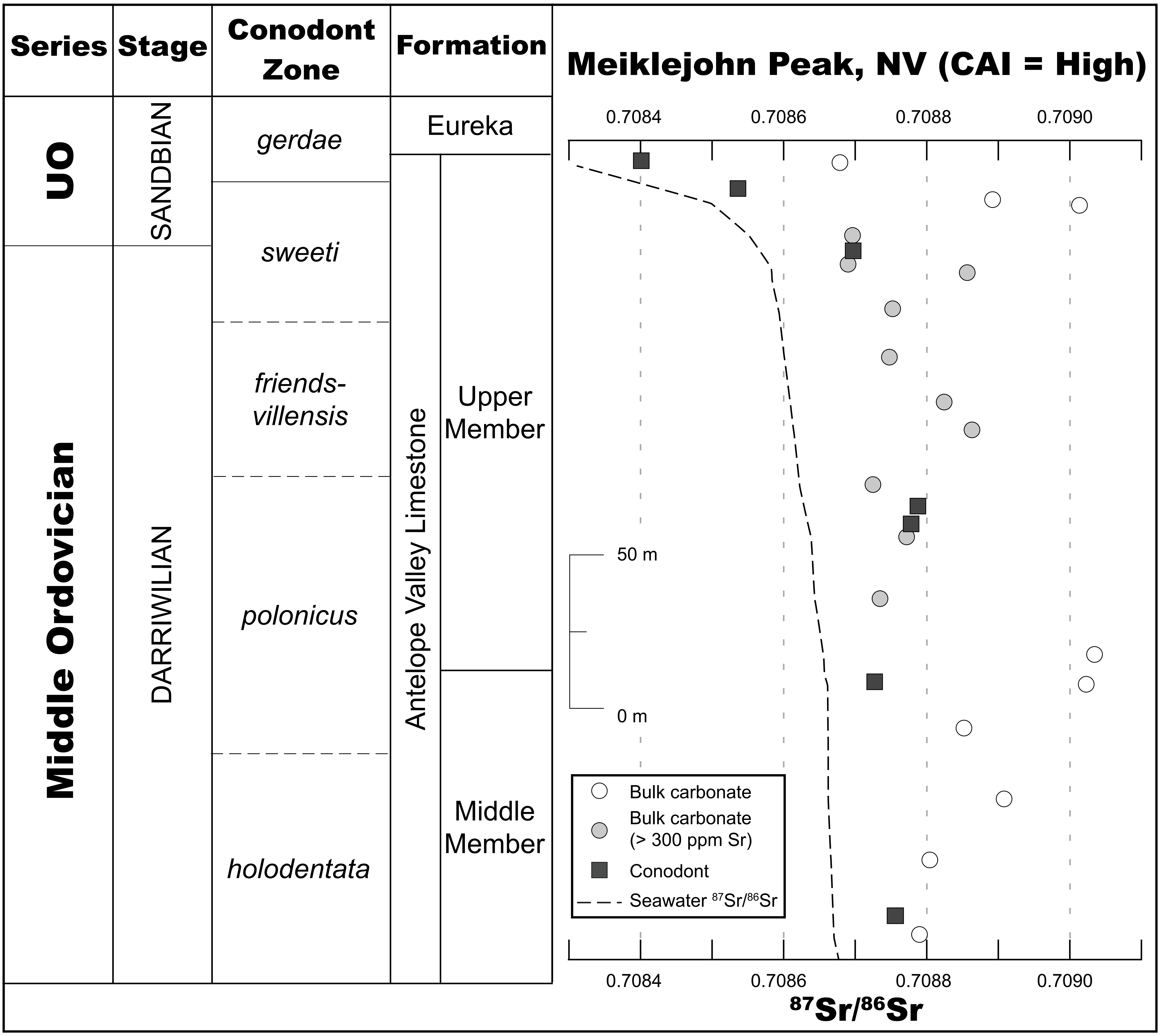

Figure DR1 - Edwards et al.

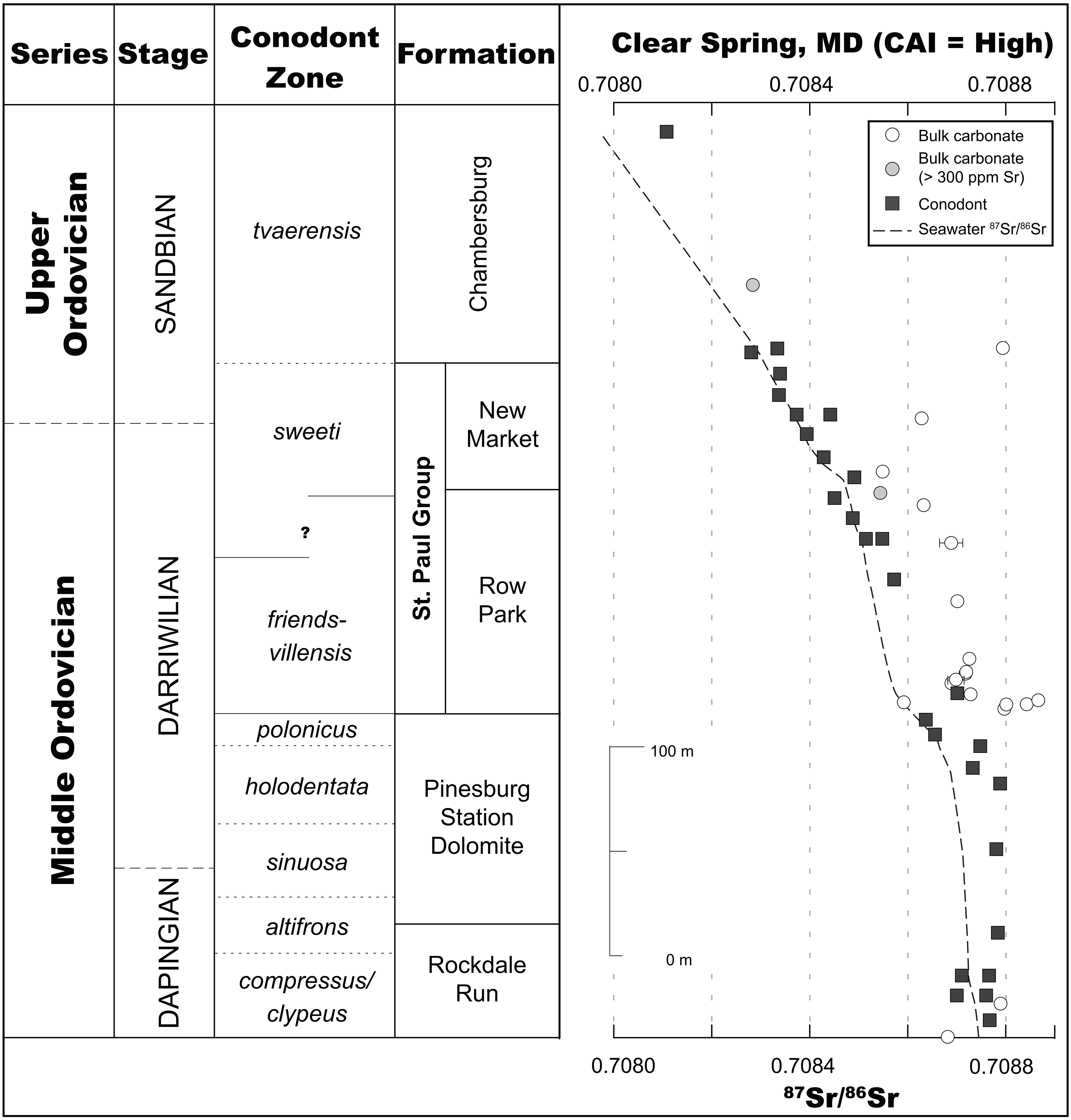

Figure DR2 - Edwards et al.

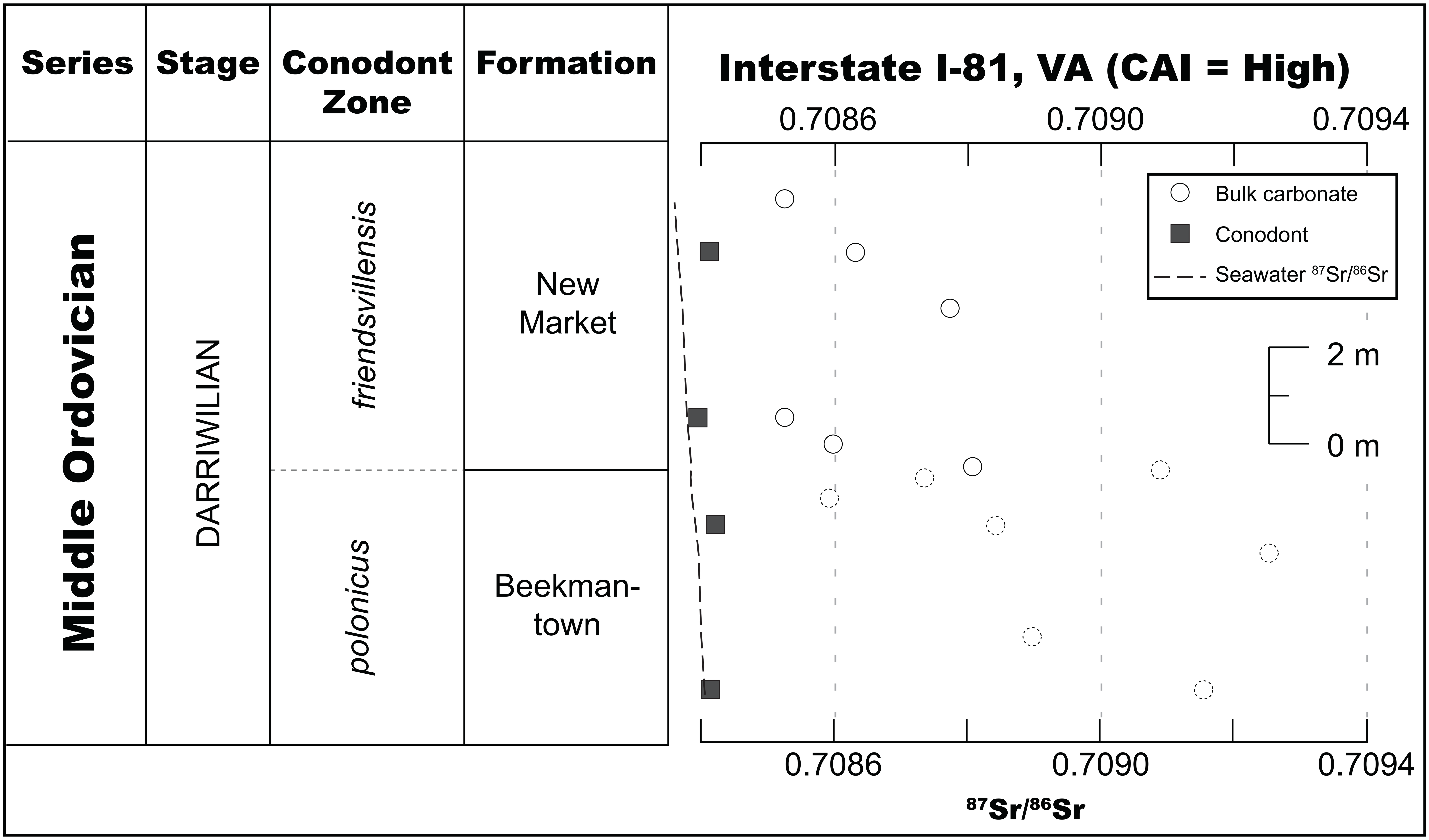

Figure DR3 - Edwards et al.

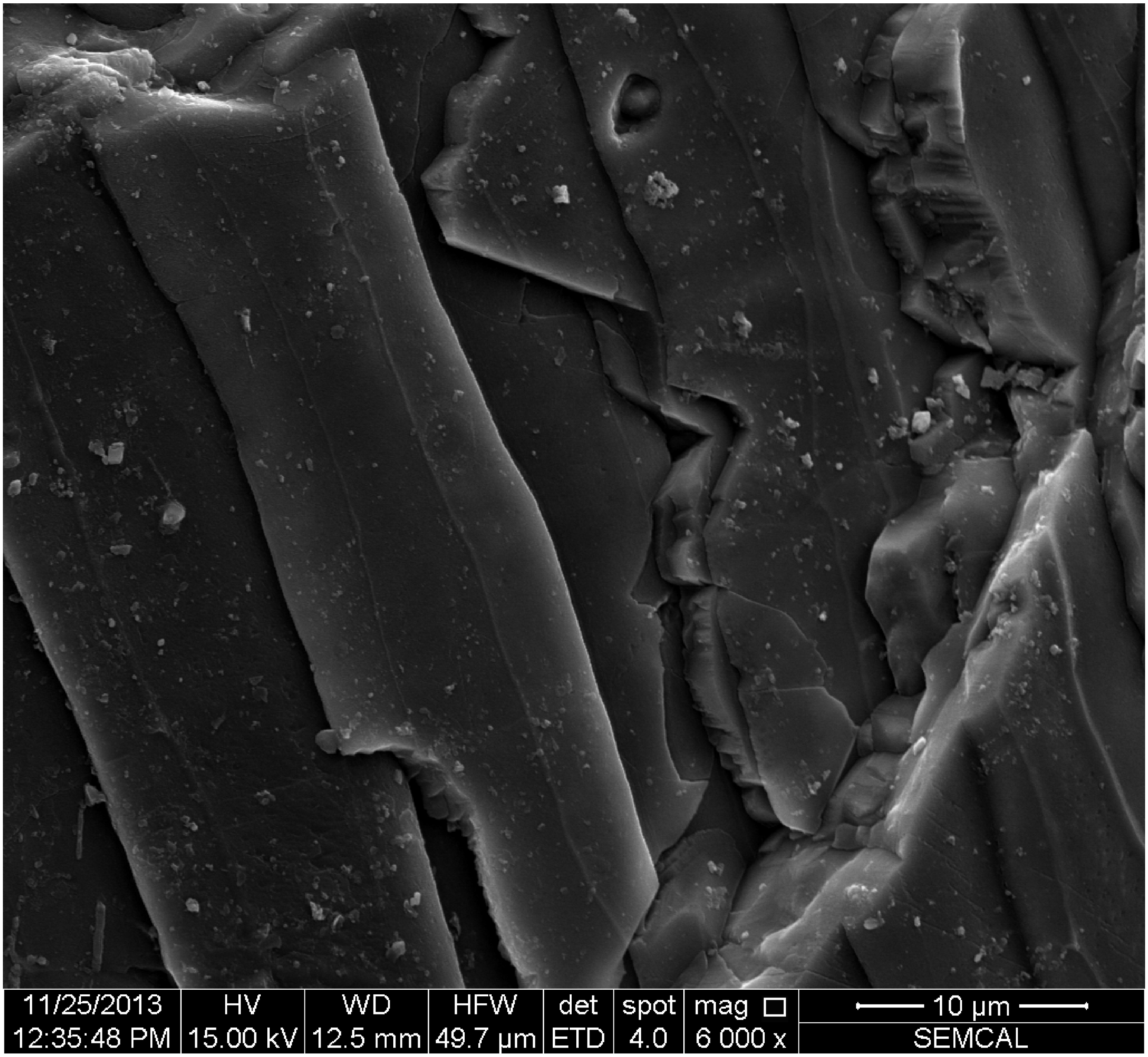

Figure DR4 - Edwards et al.

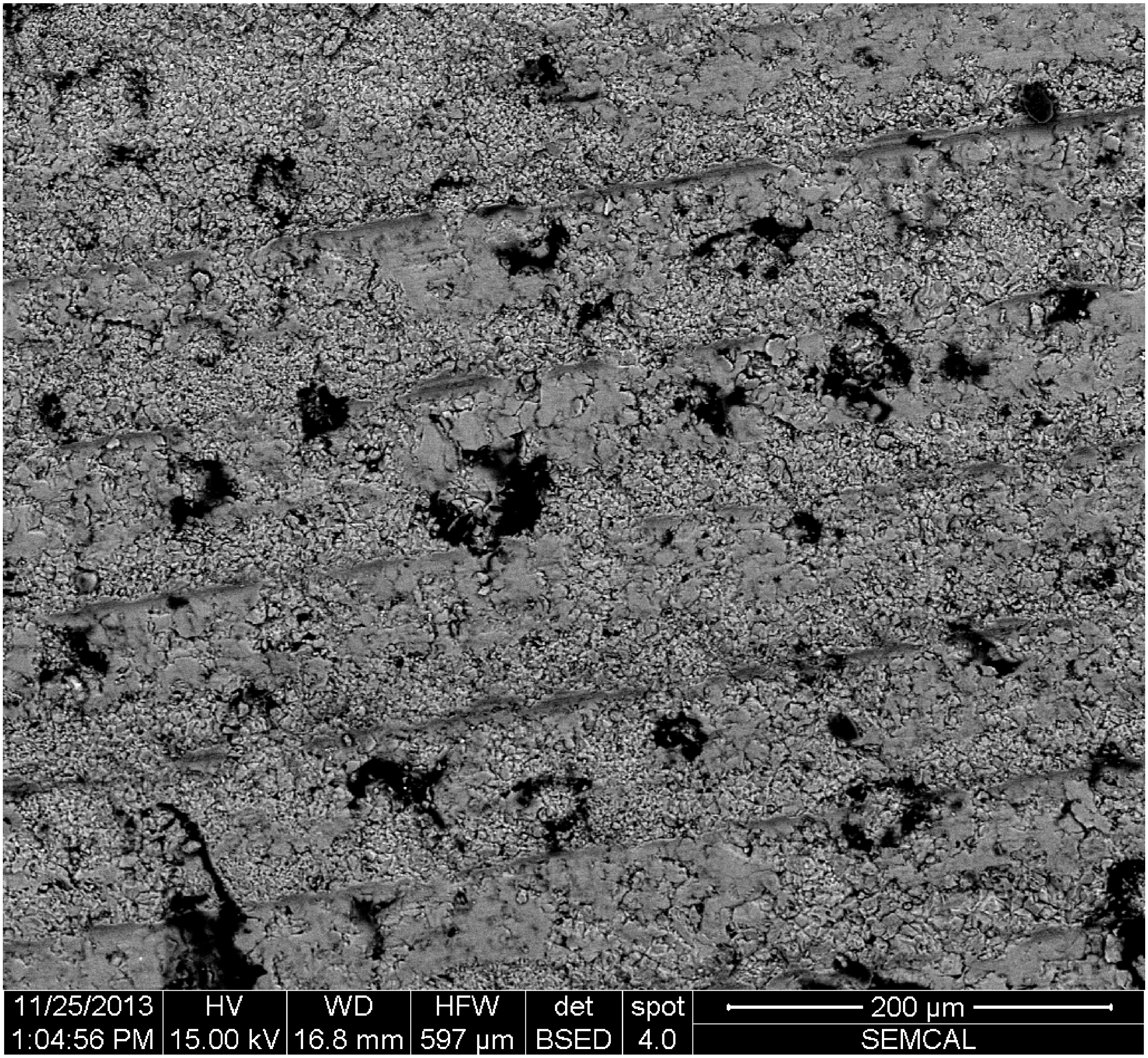

Figure DR5 - Edwards et al.

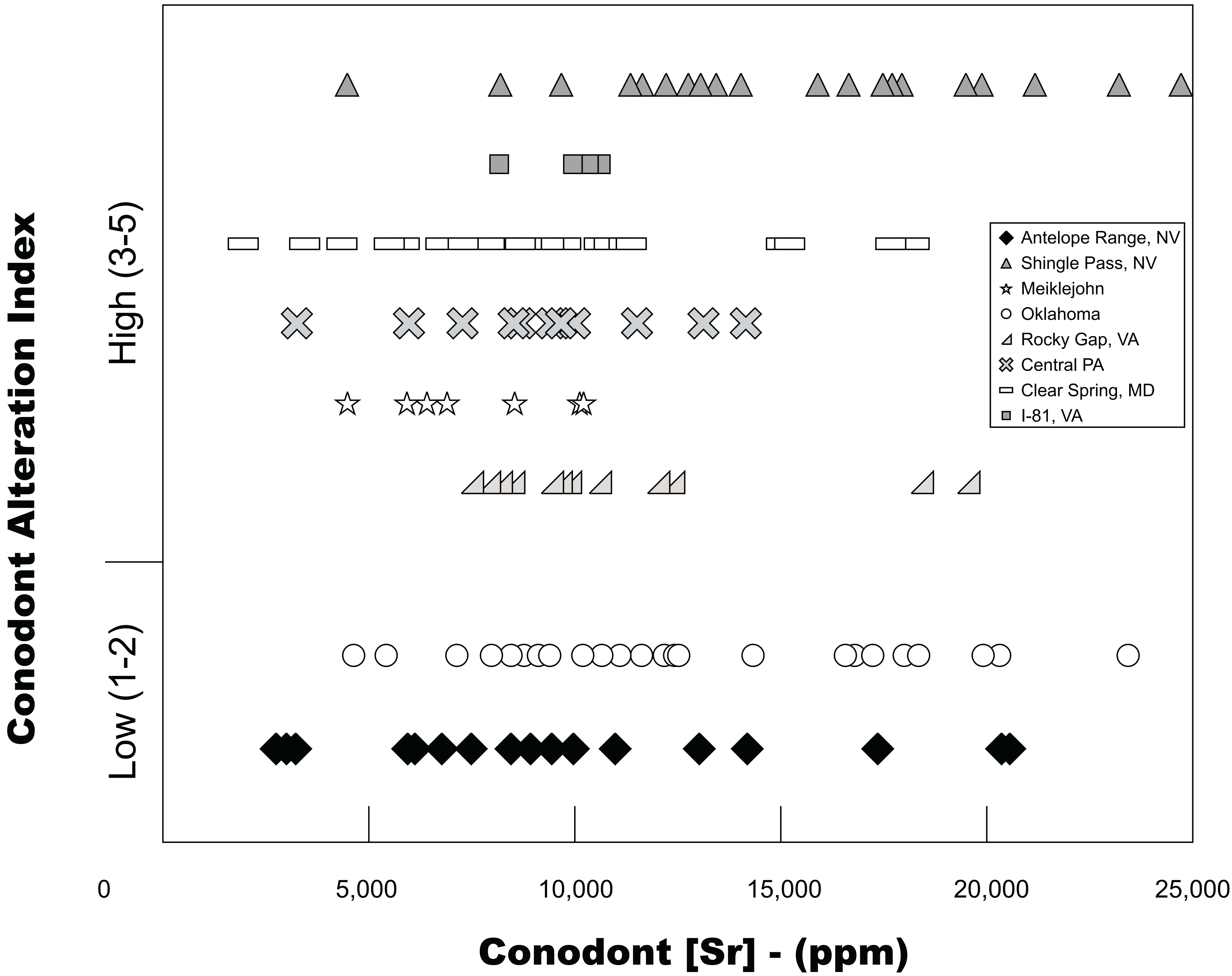

Figure DR6 - Edwards et al.

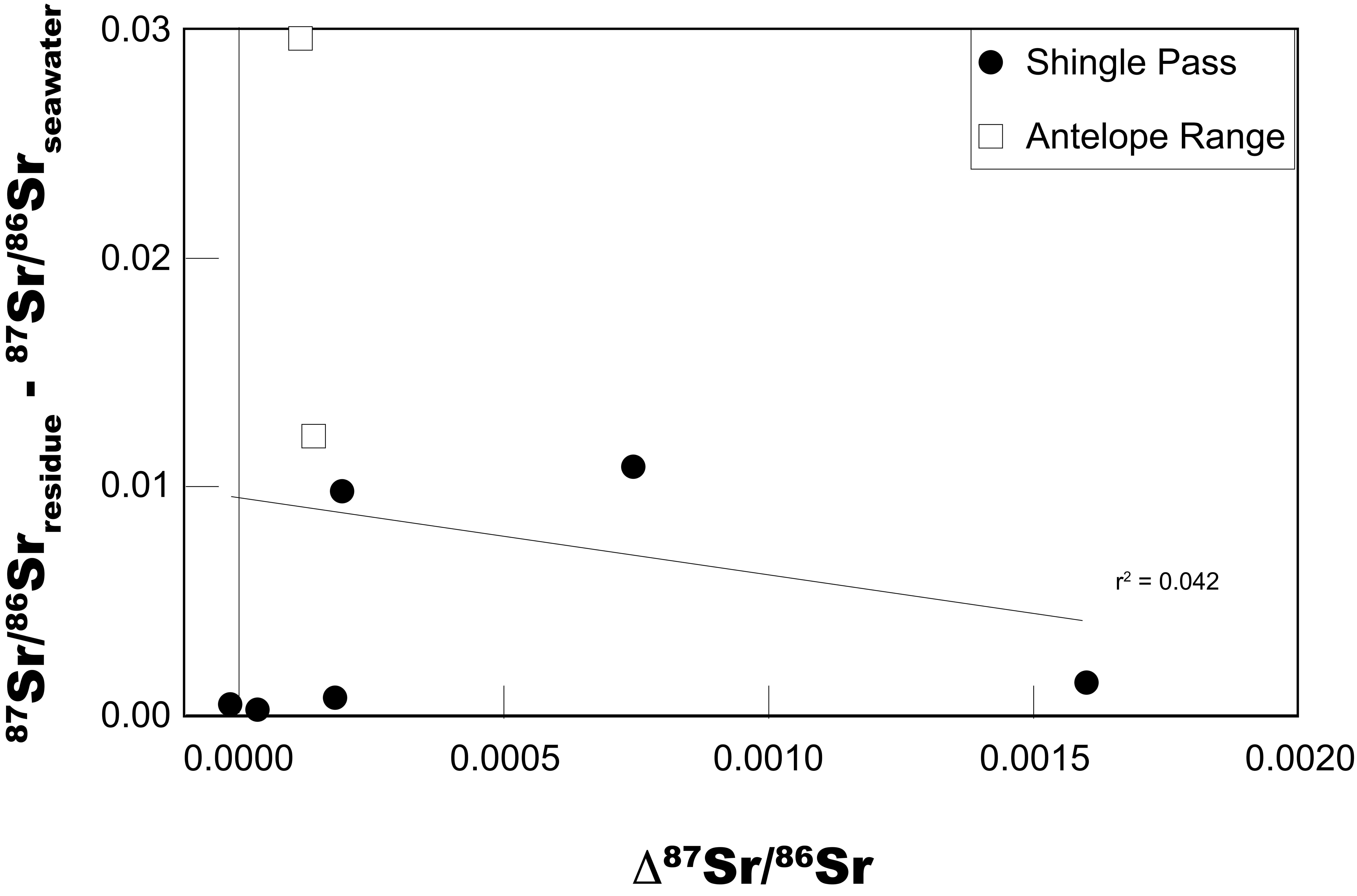

Figure DR7 - Edwards et al.

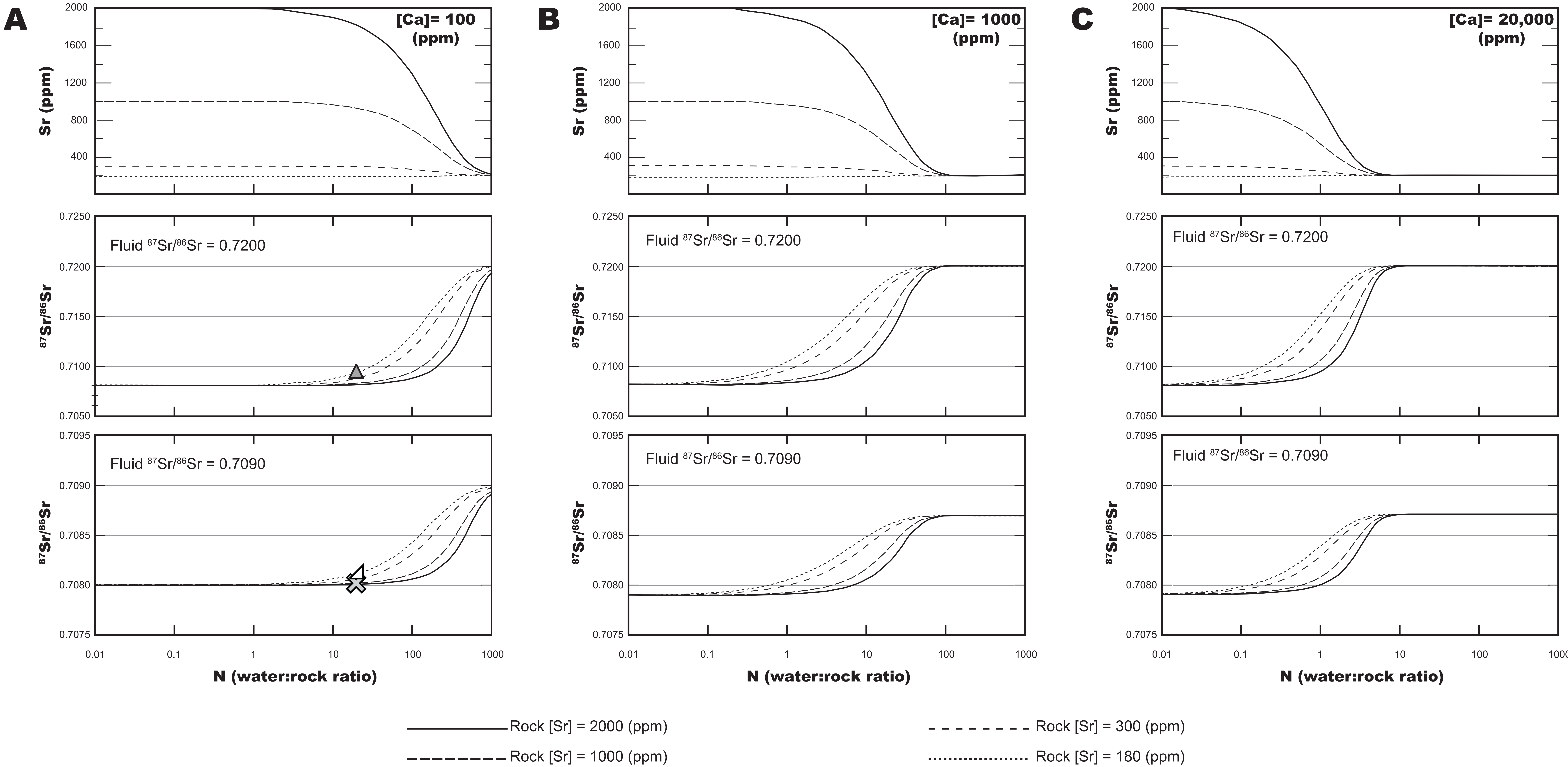

Figure DR8 - Edwards et al.